Single-element objective lens for soft x-ray differential interference contrast microscopy

Chang Chang

School of Biomedical Engineering, Science and Health Systems, Drexel University, Philadelphia, Pennsylvania 19104

Anne Sakdinawat

University of California, San Francisco—University of California, Berkeley, Joint Graduate Group in Bioengineering, Berkeley, California 94720, and Center for X-Ray Optics, Lawrence Berkeley National Laboratory, Berkeley, California 94720

Peter Fischer and Erik Anderson

Center for X-Ray Optics, Lawrence Berkeley National Laboratory, Berkeley, California 94720

David Attwood

Applied Science and Technology Graduate Group and Department of Electrical Engineering and Computer Sciences, University of California, Berkeley, California 94720, and Center for X-Ray Optics, Lawrence Berkeley National Laboratory, Berkeley, California 94720

Received February 1, 2006; accepted February 13, 2006; posted February 16, 2006 (Doc. ID 67689)

High-resolution soft x-ray differential interference contrast (DIC) imaging was demonstrated through the use of a single-element objective, the XOR pattern, in a full-field soft x-ray microscope. DIC images of the magnetic domains in a 59 nm thick amorphous $Gd_{25}Fe_{75}$ layer were obtained and magnetic phase contributions were directly imaged. With its elemental, chemical, and magnetic specificity, compatibility with various sample environments, and ease of implementation, we expect this soft x-ray DIC technique to become one of the standard modes of operation for existing full-field soft x-ray microscopes. © 2006 Optical Society of America

OCIS codes: 070.2580, 340.7460, 050.5080, 160.3820.

Nanometer resolution soft x-ray microscopy has had a major impact on nanoscience research.[1,2] The tunability to element-specific absorption edges (such as the *K*-edges of C, N, O, the *L*-edges of Ca and 3*d* transition metals, and the *M*-edges of rare-earth elements), the penetrability into water below the oxygen *K*-edge (543 eV), the polarization characteristics, and the subnanosecond time structure of soft x rays generated at synchrotron sources have leveraged soft x-ray microscopy as a powerful new tool for high-resolution imaging in biological studies, nanomagnetism, and materials sciences. A spatial resolution of 15 nm was recently demonstrated with absorption contrast as the imaging mechanism.[3] Extension to phase contrast adds another dimension to x-ray microscopy and therefore further facilitates our understanding of nanoscale phenomena. Phase contrast imaging at soft x-ray wavelengths was demonstrated by Schmahl *et al.*,[4] who used a Zernike phase plate.[5] X-ray differential interference contrast (DIC) imaging was also demonstrated,[6] followed by subsequent improvements by use of diffractive optical elements.[7,8] Here we present a novel Fourier optical element, the XOR pattern,[9] that achieves nanoscale resolution soft x-ray DIC imaging with a single-element objective lens. Unlike Zernike phase contrast, no additional optical element is needed in our experimental setup, which employs a standard soft x-ray microscope. High spatial coherence is not needed as in reciprocal space methods,[10–15] thus significantly reducing the requirements on the largely incoherent soft x-ray sources available today.

We obtain the XOR objective by combining an overlaid binary grating and a zone plate through a logical XOR operation, as shown in Fig. 1. The binary grating and zone plate are first pixelized, overlapped, and then compared pixel by pixel. At each pixel position, a logical exclusive OR (XOR) operation is performed, in which the corresponding pixel value of the resultant XOR pattern is 0 if the pixel values from the grating and the zone plate are the same and is 1 otherwise. The resultant XOR pattern effectively incorporates the function of a π-phase-shift grating into that of a zone plate. One can readily recognize the XOR objective as an altered zone plate with sections of

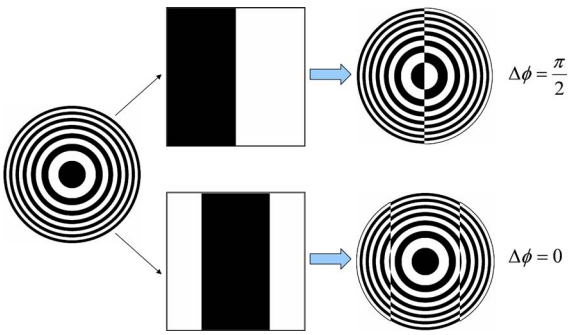

Fig. 1. (Color online) XOR objective. Bias retardation is accomplished by lateral shifting of the grating with respect to the zone plate.

0146-9592/06/101564-3/$15.00

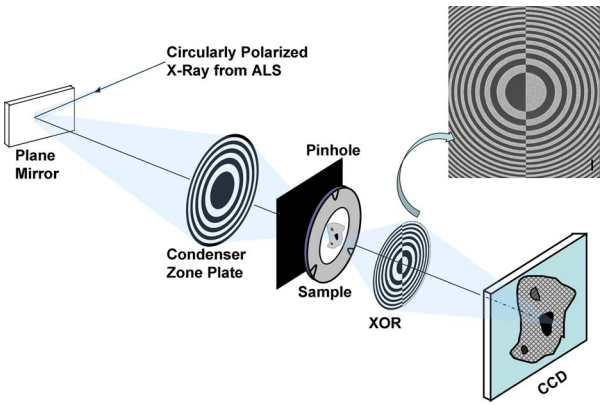

Fig. 2. (Color online) Experimental setup for soft x-ray DIC microscopy. The scanning-electron microscope photograph (inset) shows the XOR pattern with a 1 μm scale bar.

π-phase-shifted zones delineated by the overlaying grating pattern. This design also ensures that its smallest features, i.e., the critical outermost rings, typically 20 to 50 nm wide, are identical to those of a regular zone plate. Nanofabrication of this Fourier optical element is therefore compatible with the latest high-resolution overlay process used recently to produce 15 nm outermost zone width.[3]

The two characterizing properties of DIC microscopy,[16,17] lateral shear and bias retardation, are determined as follows: Noting that the π-phase-shift grating does not have a zeroth order, we find the amount of lateral shear Δx, which determines the range of spatial frequencies observable in the DIC image, as follows[9]:

$$\Delta x = 2\sin^{-1}(\lambda/d)f \approx \frac{2\Delta r D}{d}, \tag{1}$$

where Δr and D are the outermost zone width and diameter of the zone plate, respectively, λ is the wavelength, and d is the grating period. The focal length of the zone plate is given by $f=\Delta r\, D/\lambda$. In the limiting case where $d=D$, the lateral shear is $\Delta x=2\Delta r$. Because lateral shear Δx is actually independent of wavelength, the resolution of this x-ray DIC microscope remains constant across its spectral range of operation, as is the case for zone-plate-based soft x-ray microscopes. Bias retardation $2\Delta\phi$ is determined by the relative positions of the grating and the zone plate, as in the case of phase-shifting interferometry[18]:

$$\Delta\phi = 2\pi(\Delta a/d), \tag{2}$$

where Δa is the grating's relative translation in the direction of the shear with respect to its null position. For this experiment the XOR objective was designed to have diameter $D=80$ μm, outermost zone width $\Delta r=40$ nm, and grating period $d=D=80$ μm. Thus the amount of lateral shear Δx as given by Eq. (1) is 80 nm. Bias retardation $2\Delta\phi=\pi$, corresponding to a grating translation of a quarter of a period ($\Delta a = d/4$) from its null configuration, was used. Nanofabrication was conducted with a vector-scan electron-beam lithography tool, the Nanowriter.[19] The XOR objective was fabricated in 100 nm thick nickel upon a 100 nm thick silicon nitride (Si_3N_4) membrane.

The experimental setup for the soft x-ray DIC microscope is depicted in Fig. 2. In place of a Fresnel zone plate, the XOR pattern is used as the microscope objective, facilitating soft x-ray DIC microscopy by projecting two laterally shifted images onto the detector, a 1024×1024 soft x-ray sensitive CCD. All other components are identical to that of soft x-ray microscope XM-1 in its normal use at the Advanced Light Source (ALS) at Berkeley,[3] where the experiments were conducted. This soft x-ray DIC microscope, therefore, operates with the same tunable spectral range, monochromaticity ($\lambda/\Delta\lambda\sim700$), magnification, and polarization control as the XM-1 microscope. Consequently, the same elemental,[2] chemical,[20] and spin–orbit[21] specificity as the XM-1 microscope can be achieved. In addition, the versatile sample accommodation of soft x-ray microscopes also permits the examination of wet biological specimens[2] and cryogenic three-dimensional tomography[22,23] as well as nanostructured magnetic and electric samples under varying externally applied electric or magnetic fields.[24,25]

Using the XOR objective in soft x-ray microscopy, we report what we believe is the first direct imaging of magnetic phase contrast, i.e., the magnetic contribution to the real part of the refractive index, induced by x-ray magnetic circular dichroism (XMCD). XMCD introduces an additional magnetic contribution to the complex refractive index of ferromagnetic materials near (or around) the element-specific atomic resonances such as the spin–orbit coupled $L_{3,2}$ absorption edges. The relative orientation between the helicity of the circularly polarized x-ray radiation and the projection of the ferromagnetic sample's local magnetization onto the photon propagation direction determines the magnetic phase change and attenuation experienced by the transmitted x-ray radiation. These changes in complex refractive indices provide a magnetic contrast mechanism for imaging magnetic domain structures. Figure 3 shows the x-ray DIC images of a 59 nm thick amorphous $Gd_{25}Fe_{75}$ film with a pronounced perpendicular magnetic anisotropy. The probing radiation has been tuned about the L_3 and L_2 absorption edges of iron to image the local and element-specific magnetization. With a conventional objective zone plate, one can detect only the magnetic absorption contrast, which is known to vanish at photon energies below the L_3 edge and also between the

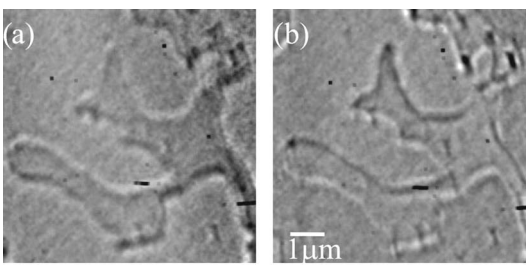

Fig. 3. DIC images of a 59 nm thick $Gd_{25}Fe_{75}$ sample obtained across the iron L_3 and L_2 edges at (a) 705 and (b) 711 eV.

L_3 and the L_2 edges.[26] Nevertheless, a magnetic phase contribution does exist at these two spectral positions [i.e., below L_3 and between L_2 and L_3 (Ref. 27)] and the XOR objective's ability to image at these two spectral positions provides an unambiguous proof of imaging with magnetic phase contrast.

Figures 3(a) and 3(b) were recorded at photon energies of 705 and 711 eV, respectively, where significant magnetic phase contrast is expected with a reversed sign. Because this x-ray DIC technique is especially sensitive to differences in complex refractive index, the resultant magnetic DIC images exhibit a magnetic contrast at the boundaries of the magnetic domains, i.e., the domain wall regions, where the magnetization changes its direction. As a result, the magnetic phase effect appears as an inversion of the dark–light regions near the magnetic domain boundaries. This causes the bas-relief pattern to switch from above to below the nominal surface. For comparison, absorption contrast soft x-ray microscopy images of the identical sample, obtained with a conventional zone plate objective, were published earlier.[28] In comparison with existing magnetic imaging techniques based on XMCD,[21,28,29] this x-ray DIC microscope is especially suitable to image, with high spatial resolution, regions of spin inhomogeneities such as the magnetic domain walls, and we therefore anticipate that this capability will permit further detailed analysis of these actively researched areas.[29,30]

A new form of soft x-ray DIC microcopy that uses an XOR objective lens opens a new dimension in nanoscale imaging in which direct phase contrast is observed. We anticipate its use in both magnetic and biological studies, for which nanoscale phase effects are of great scientific interest. We also expect it to become a standard mode of operation in existing full-field soft x-ray microscopes. Future improvement in spatial resolution with smaller, 10–15 nm outermost zone widths[3] is also anticipated. Further extension, to harder x rays, with advantages accrued by decreased absorption, is anticipated with future development of thick, high aspect ratio zone plates and XOR patterns.

The authors acknowledge support from Commonwealth of Pennsylvania Department of Health's Health Research Formula Fund, the National Science Foundation's Engineering Research Center Program, and the Department of Energy's Office of Science, Office of Basic Energy Sciences. C. Chang's email address is chang.chang@drexel.edu.

References

1. J. Susini, D. Joyeux, and F. Polack, eds., *X-Ray Microscopy VII* (EDP Sciences, Paris, 2003).
2. D. T. Attwood, *Soft X-Rays and Extreme Ultraviolet Radiation* (Cambridge U. Press, 1999).
3. W. L. Chao, B. Harteneck, J. Liddle, E. Anderson, and D. T. Attwood, Nature **435**, 1210 (2005).
4. G. Schmahl, D. Rudolph, G. Schneider, P. Guttmann, and B. Niemann, Optik (Stuttgart) **97**, 181 (1994).
5. F. Zernike, Physica (The Hague) **9**, 686 (1942).
6. T. Wilhein, B. Kaulich, E. Di Fabrizio, F. Romanato, S. Cabrini, and J. Susini, Appl. Phys. Lett. **78**, 2082 (2001).
7. E. Di Fabrizio, D. Cojoc, S. Cabrini, B. Kaulich, J. Susini, P. Facci, and T. Wilhein, Opt. Express **11**, 2278 (2003).
8. U. Vogt, M. Lindblom, P. Jansson, T. Tuohimaa, A. Holmberg, H. Hertz, M. Wieland, and T. Wilhein, Opt. Lett. **30**, 2167 (2005).
9. C. Chang, E. Anderson, P. Naulleau, E. Gullikson, K. Goldberg, and D. Attwood, Opt. Lett. **27**, 1028 (2002).
10. I. McNulty, J. Kirz, C. Jacobsen, E. Anderson, M. Howells, and D. Kern, Science **256**, 1009 (1992).
11. S. Eisebitt, J. Lüning, W. Schlotter, M. Lorgen, O. Hellwig, W. Eberhardt, and J. Stöhr, Nature **432**, 885 (2004).
12. J. W. Miao, P. Charalambous, J. Kirz, and D. Sayre, Nature **400**, 342 (1999).
13. D. Shapiro, P. Thibault, T. Beetz, V. Elser, M. Howells, C. Jacobsen, J. Kirz, E. Lima, H. Miao, A. Neiman, and D. Sayre, Proc. Natl. Acad. Sci. U.S.A. **102**, 15343 (2005).
14. H. N. Chapman, A. Barty, S. Marchesini, A. Noy, S. P. Hau-Riege, C. Cui, M. R. Howells, R. Rosen, H. He, J. C. H. Spence, U. Weierstall, T. Beetz, C. Jacobsen, and D. Shapiro, "High-resolution *ab initio* three-dimensional x-ray diffraction microscopy," J. Opt. Soc. Am. A (to be published).
15. D. Paganin and K. A. Nugent, Phys. Rev. Lett. **80**, 2586 (1998).
16. G. Nomarski, J. Phys. Radium **16**, 9S (1955).
17. C. J. Cogswell and C. J. R. Sheppard, J. Microsc. **165**, 81 (1992).
18. D. Malacara, *Optical Shop Testing* (Wiley, 1992).
19. E. H. Anderson, D. Olynick, B. Harteneck, E. Veklerov, G. Denbeaux, W. Chao, A. Lucero, L. Johnson, and D. Attwood, J. Vac. Sci. Technol. B **18**, 2970 (2000).
20. H. Ade, X. Zhang, S. Cameron, C. Costello, J. Kirz, and S. Williams, Science **258**, 972 (1992).
21. P. Fischer, G. Schütz, G. Schmahl, P. Guttmann, and D. Raasch, Z. Phys. B: Condens. Matter **101**, 313 (1996).
22. G. Schneider, E. Anderson, S. Vogt, C. Knochel, D. Weiss, M. Legros, and C. Larabell, Surf. Rev. Lett. **9**, 177 (2002).
23. C. Larabell and M. Le Gros, Mol. Biol. Cell **15**, 957 (2004).
24. P. Fischer, G. Denbeaux, T. Ono, T. Okuno, T. Eimüller, D. Goll, and G. Schütz, J. Phys. D **35**, 2391 (2002).
25. G. Schneider, G. Denbeaux, E. Anderson, B. Bates, A. Pearson, M. Meyer, E. Zschech, D. Hambach, and E. Stach, Appl. Phys. Lett. **81**, 2535 (2002).
26. C. T. Chen, F. Sette, Y. Ma, and S. Modesti, Phys. Rev. B **42**, 7262 (1990).
27. J. Kortright and S. Kim, Phys. Rev. B **62**, 12216 (2000).
28. P. Fischer, T. Emüller, G. Schütz, and G. Denbeaux, Struct. Chem. **14**, 39 (2003).
29. J. Stöhr, Y. Wu, B. Hermsmeier, M. Samant, G. Harp, S. Koranda, D. Dunham, and B. Tonner, Science **259**, 658 (1993).
30. D. A. Allwood, G. Xiong, C. Faulkner, D. Atkinson, D. Petit, and R. Cowburn, Science **309**, 1688 (2005).